Journal of Neurotrauma
40:1112–1129 (June 2023)

DOI: 10.1089/neu.2022.0220

Journal of Neurotrauma

ORIGINAL ARTICLE IMAGING

Assessing Pediatric Mild Traumatic Brain Injury and Its Recovery Using Resting-State Magnetoencephalography Source Magnitude Imaging and Machine Learning

Ming-Xiong Huang,[1,2] Annemarie Angeles-Quinto,[1,2] Ashley Robb-Swan,[1,2] Bianca G. De-la-Garza,[3] Charles W. Huang,[4] Chung-Kuan Cheng,[5] John R. Hesselink,[1] Erin D. Bigler,[6] Elisabeth A. Wilde,[6] Florin Vaida,[7] Emily A. Troyer,[3] and Jeffrey E. Max[3,8,*]

Abstract

The objectives of this machine-learning (ML) resting-state magnetoencephalography (rs-MEG) study involving children with mild traumatic brain injury (mTBI) and orthopedic injury (OI) controls were to define a neural injury signature of mTBI and to delineate the pattern(s) of neural injury that determine behavioral recovery. Children ages 8-15 years with mTBI ($n = 59$) and OI ($n = 39$) from consecutive admissions to an emergency department were studied prospectively for parent-rated post-concussion symptoms (PCS) at: 1) baseline (average of 3 weeks post-injury) to measure pre-injury symptoms and also concurrent symptoms; and 2) at 3-months post-injury. rs-MEG was conducted at the baseline assessment. The ML algorithm predicted cases of mTBI versus OI with sensitivity of $95.5 \pm 1.6\%$ and specificity of $90.2 \pm 2.7\%$ at 3-weeks post-injury for the combined delta-gamma frequencies. The sensitivity and specificity were significantly better ($p < 0.0001$) for the combined delta-gamma frequencies compared with the delta-only and gamma-only frequencies. There were also spatial differences in rs-MEG activity between mTBI and OI groups in both delta and gamma bands in frontal and temporal lobe, as well as more widespread differences in the brain. The ML algorithm accounted for 84.5% of the variance in predicting recovery measured by PCS changes between 3 weeks and 3 months post-injury in the mTBI group, and this was significantly lower ($p < 10^{-4}$) in the OI group (65.6%). Frontal lobe pole (higher) gamma activity was significantly ($p < 0.001$) associated with (worse) PCS recovery exclusively in the mTBI group. These findings demonstrate a neural injury signature of pediatric mTBI and patterns of mTBI-induced neural injury related to behavioral recovery.

Keywords: delta rhythm; gamma rhythm; machine learning; pediatric traumatic brain injury; resting-state MEG

[1]Department of Radiology, University of California, San Diego, California, USA.
[2]Radiology and Research Services, VA San Diego Healthcare System, San Diego, California, USA.
[3]Department of Psychiatry, University of California, San Diego, California, USA.
[4]Department of Bioengineering, Stanford University, Stanford, California, USA.
[5]Department of Computer Science and Engineering, University of California, San Diego, California, USA.
[6]Department of Neurology, University of Utah, Salt Lake City, Utah, USA.
[7]Herbert Wertheim School of Public Health, Division of Biostatistics and Bioinformatics, University of California, San Diego, California, USA.
[8]Department of Psychiatry, Rady Children's Hospital, San Diego, California, USA.

*Address correspondence to: *Jeffrey E. Max, MBBCh, Department of Psychiatry, University of California, San Diego, 5755 Oberlin Drive, Suite 301, San Diego, CA 92121, USA*
E-mail: jmax@health.ucsd.edu

Introduction

Traumatic brain injury (TBI) in children and adolescents is a major public health problem. The Centers for Disease Control and Prevention reported approximately 640,000 pediatric TBI-related emergency department (ED) visits among children 14 years of age and younger in 2013,[1,2] with most TBIs (70-90%) falling in the mild range of severity.[3,4]

Behavioral and psychiatric studies of pediatric mild TBI (mTBI),[5,6] with some exceptions,[7-9] have demonstrated a significant increase in symptoms and disorders, respectively, in the first 3 months post-injury compared with non-brain-injured age- and sex-matched controls (e.g., children with orthopedic fractures). These findings are driven by a minority of children with mTBI (10-23%),[6,10-12] who constitute an important group worthy of study in efforts to mitigate suffering on an individual basis as well on an epidemiological basis due to the prevalence of mTBI. Investigations of mTBI by our group[6,13] and others[5,12] have been guided by a biopsychosocial model approach.[14] In contrast, the current study focused on a biological approach and by utilizing resting-state magnetoencephalography (rs-MEG), attempted to address two overarching questions: 1) What is a neural injury signature of pediatric mTBI (i.e., how can the brains of patients with mTBI be distinguished from patients with non-brain orthopedic injury?); and 2) What pattern(s) of neural injury determine behavioral recovery from early post-injury to sub-acute outcome (e.g., 3 months post-injury)?

With regard to the question about a neural injury signature of pediatric mTBI, studies utilizing magnetic resonance imaging (MRI) in children with mTBI have yielded mixed results. Longitudinal morphometric studies specific to mTBI in children are limited, but suggest the potential for persistent alteration following injury.[15-17] Other structural imaging techniques such as diffusion imaging have been conducted because diffuse axonal injury (DAI) is known to play a major role in brain dysfunction, producing an imbalance in excitatory/inhibitory neural activity after mTBI.[18] It is widely assumed that white matter tracts are primarily vulnerable to DAI, which causes cortical network disconnection.[19,20]

However, diffusion imaging results are variable for pediatric mTBI.[21] In the acute to sub-acute post-injury interval, group differences have been reported in commonly used metrics such as fractional anisotropy (FA) and mean diffusivity in select white matter tracts,[16,17,22–35] as well as global and regional disruption to structural network connectivity,[36,37] though others report no difference for those with mTBI.[38–42] Results of longitudinal diffusion imaging studies in pediatric mTBI also reflect mixed results, with some reflecting resolution of change over time,[43,44] and others reflecting increased or persistent differences following injury.[17,27,42,45] Studies assessing resting-state function via functional MRI (fMRI) after childhood TBI are limited and almost exclusively cross-sectional, but they generally demonstrate persistent alterations in the functional connectivity of multiple resting-state networks even in mTBI.[46–49]

In our preliminary study,[50] we utilized a different functional imaging technique (i.e., rs-MEG). rs-MEG source imaging in the children with mTBI, in contrast to control participants, showed: 1) bilateral insular cortices hyperactivity in alpha, beta, and low-frequency bands, left amygdala hyperactivity in alpha band, and hyperactivity from left precuneus in beta band; and 2) bilateral dorsolateral prefrontal cortices hypoactivity in alpha and beta bands, hypoactivity from ventromedial prefrontal cortex in beta band, hypoactivity from ventrolateral prefrontal cortex in gamma band, hypoactivity from anterior cingulate cortex in alpha band, and hypoactivity from right precuneus in alpha band.

There are limited data related to the second question about pattern(s) of neural injury that determine behavioral recovery from early post-injury to sub-acute outcome. A study examining microstructural white matter differences found that quicker resolution of post-concussion symptoms (PCS) and return to play in adolescent football players was related to higher FA in the inferior longitudinal fasciculus, inferior fronto-occipital fasciculus, and uncinate fasciculus.[51] In another study, lower FA in the uncinate fasciculus was associated with persistent PCS.[26] Other biologically-related variables such as severity of injury (more severe type of mTBI), repeated mTBI, and inpatient hospitalization for the injury, increase the risk of behavioral and psychiatric sequelae.[52] A study of consecutively hospitalized children with mTBI, most of whom had a lesion detected on a research MRI, found that frontal white matter (network) lesions were significantly associated with novel psychiatric disorders in the first 6 months post-injury.[13] However, the vast majority of pediatric mTBI patients are treated in the ED, are not hospitalized, and very few have lesions demonstrated on MRI.[5,53]

As reviewed above, the state of the science with regard to defining a neural signature of mTBI and clarifying pattern(s) of neural injury that determine behavioral recovery from early post-injury to sub-acute outcome, is at an early stage of investigation. Traditional MRI techniques have been relatively insensitive to the effects of mTBI, while diffusion MRI focused on microstructural white matter has shown interesting, but mixed, results. Many of the knowledge lacunae may be filled by utilizing MEG. Consistent with our preliminary study of pediatric mTBI,[50] adult mTBI studies have uniformly demonstrated that MEG is a highly sensitive technology in terms of detecting evidence of gray matter (GM) injury.[54–60]

The possibility that GM pathologies following mTBI are at play was suggested by an animal study showing that DAI substantially alters the integrity of GM.[61] In

this regard, MEG source imaging can detect subtle pathology that often goes undetected in individuals with mTBI when using structural neuroimaging techniques.[55,56,62] MEG directly measures the magnetic signal due to neuronal activation in GM with high spatial localization accuracy (2-3 mm in cortex)[63] and high temporal resolution (< 1 msec), which translates into excellent frequency specificity at different frequency bands.[64] Regional resting state (rs-MEG) slow-wave (delta band 1-4 Hz, extending to theta band 5-7 Hz) markers are highly sensitive in distinguishing patients with chronic and sub-acute mTBI with persistent PCS on a single-subject basis from neurologically intact individuals.[55,56,62,65,66] Abnormal slow-waves have also been reported in a cohort consisting of acute, sub-acute, and participants with chronic mTBI.[57]

We also discovered that rs-MEG gamma-band (30-80 Hz) markers showed striking hyperactivity in adults with combat-related mTBI.[67] In addition, task-evoked MEG recordings during working memory detected abnormal alpha, beta, and gamma signals throughout the brain in adults with combat-related mTBI, which correlated with poorer cognitive functioning.[68] However, the vast number of markers of aberrant neuronal function throughout the brain poses a significant challenge for clinical applications. In this regard, analytic approaches, such as machine learning (ML) are needed to discover optimal combinations of aberrant features across different frequency bands that best distinguish mTBI and also predict neurobehavioral recovery, especially for the pediatric population, which is virtually unstudied.

ML is a data-driven approach that optimally integrates high-dimensional features in large datasets. It has been used to classify mTBI and healthy control (HC) participants based on rs-MEG phase-synchronization analyses of functional connectivity. For example, Vakorin and colleagues applied a support vector machine (SVM) classifier to rs-MEG source-based measures of simple functional connectivity, reporting that reduced delta and gamma connectivity, together with increased alpha-band connectivity, distinguished civilian patients with mTBI from HCs with 88% accuracy.[69] Dimitriadis and colleagues[70] applied an extreme learning machine classifier to rs-MEG sensor-based functional connectivity measures derived from graph theory to measure the overall efficiency of information transfer across the brain and at local levels. They reported that alpha-band local efficiency distinguished civilian patients with mTBI from HCs with 100% accuracy.[70] These studies illustrate the great potential of ML approaches to uncover optimal combinations of discriminating features, which can streamline the interpretation of analyses from high-dimensional data. Despite the very good to excellent classification accuracies reported in these studies, functional connectivity metrics do not always easily pinpoint the injured brain regions due to the involvement of multiple regions in functional connectivity analysis and the many interconnecting pathways that connect these regions.

Our focus was to examine a ML model using acute/sub-acute rs-MEG data for: 1) accurately classifying pediatric mTBI and orthopedic injury (OI); and 2) predicting PCS recovery. We investigated the performances of rs-MEG ML when modeling individual delta- or gamma-band and when both bands were combined (i.e., both-band model). This strategy was to determine if regional changes in one or more frequency bands optimally distinguished participants with mTBI and OI. Further, we evaluated the spatial differences of rs-MEG data using the conventional voxel-wise group statistical analysis. In addition, we studied some regional rs-MEG features or classifiers by correlating them with measures of PCS recovery.

The hypotheses underlying this investigation were as follows:

- Hypothesis 1a: The ML algorithm using post-injury rs-MEG data will predict cases of mTBI versus OI with sensitivity and specificity both over 90% at 3 weeks post-injury. The predictive performance will improve significantly when data from rs-MEG delta (1-4 Hz) and gamma (30-80 Hz) frequency bands are integrated. Hypothesis 1b: We predicted that spatial differences in rs-MEG activity between mTBI and OI groups will involve both delta and gamma bands in disparate brain regions, particularly in frontal lobe poles.
- Hypothesis 2: A ML algorithm with post-injury rs-MEG data will explain >80% of variance in predicting the recovery as measured by PCS changes between 3 weeks post-injury and the 3-month exams in the mTBI group. The predictive performance will be significantly lower in the OI group.

Methods

Research participants

Study participants included 98 children, age 8 to 15 years, consecutively treated at the ED at Rady's Children's Hospital, San Diego, for either a mTBI or OI. Inclusion criteria for the mTBI group were: 1) evidence of a TBI that resulted in an observed loss of consciousness; 2) a Glasgow Coma Scale (GCS)[71] score of 13-14; or 3) a GCS score of 15 with at least two symptoms of concussion as noted by the ED medical staff (e.g., persistent post-traumatic amnesia, transient neurological deficits, vomiting, nausea, headache, diplopia, dizziness).

Exclusion criteria for the mTBI group included: 1) loss of consciousness greater than 30 min or a GCS score of less than 13; 2) any injury requiring neurosurgical intervention; 3) documented history of previous TBI meeting the above criteria for at least mTBI; 4) associated injury

that is severe, documented with the Abbreviated Injury Scale (AIS)[72] score greater than 3; 5) hypoxia, hypotension, or shock associated with the injury; 6) associated injury that is likely to interfere with cognitive testing (e.g., injury to dominant upper limb); 7) alcohol or drug ingestion involved with the injury; 8) pre-injury neurological disorder, schizophrenia, autism spectrum disorder, or intellectual deficiency; 9) any medical contraindication to MRI and MEG; 10) illegal immigrant status; 11) history of child abuse; 12) extensive dental hardware or orthodontia (e.g., braces and large metal dentures; fillings were acceptable) or other metal objects in the head, neck, or face areas that cause artifacts in the MEG data, not removable during pre-processing; and 13) currently taking medications (e.g., some sedative neuroleptics and hypnotics) known to alter the power of brain rhythms.[73]

Inclusion criterion for the OI group was the presence of upper or lower limb fractures. Exclusion criteria for the OI group included: 1) injury to the head or TBI; and 2) exclusion criteria 3 through 13 for the mTBI group above. Determination of eligibility was made by review of the electronic medical record and screening interview with the parent/guardian.

Participants were invited to attend three research sessions at different time-points: 1) at baseline (approximately 3 weeks post-injury); 2) at MRI (approximately 7 weeks post-injury); and 3) at 3-month follow-up. Entry criteria were specified with respect to the initial ED visit regardless of symptom status at the baseline or subsequent visits.

Post-concussive symptom assessment

During the baseline and 3-month follow-up sessions, parents rated PCS on the Health and Behavior Inventory (HBI) scale,[74] which is comprised of 20 items that assess cognitive ($n=11$) and somatic ($n=9$) symptoms that have been related to TBI. The 11 cognitive symptoms include problems with attention, distractibility, concentration, memory, following directions, daydreaming, confusion, forgetfulness, task completion, problem solving, and learning. The nine somatic symptoms were headaches, dizziness, the feeling of a spinning room, faintness, blurred vision, double vision, nausea, commonly fatigued, and easily fatigued. The frequency of each symptom is rated on a four-point scale ranging from 0 (''never''), 1 (''rarely''), 2 (''sometimes''), and 3 (''often''). Thus, the ranges of the HBI domain scores are from 0-33, 0-27, and 0-60 for cognitive, somatic, and total score, respectively. The scale has been used and has been recommended for use in research in pediatric TBI studies.[74,75] Factor analyses demonstrated dimensions representative of cognitive and somatic symptoms. The HBI has adequate construct validity, good to excellent internal consistency, and reliability, and can be used in longitudinal assessments of children.[76] The parent-rated version rather than the child-rated version of the HBI was used for these analyses because the parent may be in the best observational role to rate symptoms following injury.[77] Parents rated their child's somatic and cognitive symptoms during the 1-month interval prior to the injury, the week of baseline (acute/sub-acute visit), and the week of the 3-month follow-up. The severity of cognitive, somatic, and total symptoms is calculated by summing the scores in each domain.

MEG data acquisition and signal pre-processing

rs-MEG data were collected at the University of California, San Diego MEG Center using the VectorView™ whole-head MEG system (Elekta-Neuromag, Helsinki, Finland) with 306 MEG channels. The rs-MEG exam was conducted during the acute/sub-acute baseline post-injury visit. Participants sat inside a multi-layer magnetically-shielded room.[78] MEG recordings were divided into two 5-min blocks where the participant was instructed to keep his/her eyes closed and empty his/her mind. Data were sampled at 1000 Hz and run through a high-pass filter with a 0.1 Hz cut-off, and a low-pass filter with a 330 Hz cut-off. Micro eye blinks and eye movements were monitored using two pairs of bipolar electrodes, and heart signals were monitored with another pair of bipolar electrodes.

Substantial efforts were taken to help ensure that participants were alert during the rs-MEG recordings. Prior to MEG sessions, participants completed a questionnaire about the number of hours they slept the previous night, how rested they felt, and if there was any reason that they might not be attentive and perform to the best of their abilities (e.g., headache, pain). Sessions alternated between eyes-closed and eyes-open conditions, and eye blinking and movement were monitored. During MEG recording, participants were viewed on camera and technicians continuously monitored alpha band oscillations, which are consistently associated with tonic alertness.[79]

Pre-processing steps to remove artifacts and noises in rs-MEG data

Eyes-closed rs-MEG sensor waveforms were first run through MaxFilter, also known as signal space separation,[80-82] to remove external interferences (e.g., magnetic artifacts due to metal objects, strong cardiac signals, environment noises) and to co-register the MEG data by removing the small head movements across the two 5-min eyes-closed sessions. Residual artifacts near the sensor array due to micro eye movements and residual cardiac signals were removed via Independent Component Analysis using Fast-ICA.[83,84] The waveforms associated with top independent components were examined by an experienced MEG data analyst,

along with eye and heart signals. Independent components associated with eye movement, heartbeats, and other artifacts were removed.

Structural MRI, MEG-MRI registration, boundary element method forward calculation

Structural MRI of the participant's head was collected using a General Electric 3T MRI scanner. The acquisition contains a standard high-resolution anatomical volume with a resolution of $0.94 \times 0.94 \times 1.2\,mm^3$ using a T1-weighted three-dimensional inversion recovery prepared fast spoiled gradient recalled (3D-IR-FSPGR) pulse sequence. Scanner-related non-linear imaging distortions were corrected using a gradient non-linearity correction approach.[85] To co-register the MEG with MRI coordinate systems, three anatomical landmarks (i.e., left and right pre-auricular points and nasion) were measured for each participant using the Probe Position Identification system (Polhemus, USA). By using MRILAB (Elekta/Neuromag) to identify the same three points on the participant's magnetic resonance (MR) images, a transformation matrix involving both rotation and translation between the MEG and MR coordinate systems was generated. To increase the reliability of the MEG-MR co-registration, approximately 120 points on the scalp were digitized with the Polhemus system, in addition to the three landmarks, and those points were co-registered onto the scalp surface of the MR images.

The T1-weighted images were also used to extract the brain volume and innermost skull surface (SEGLAB software by Elekta/Neuromag). The Realistic Boundary Element Method (BEM) head model was used for MEG forward calculation.[86,87] The BEM mesh was constructed by tessellating the inner skull surface from the T1-weighted MRI into $\sim$6000 triangular elements with $\sim$5 mm size. A cubic source grid with 5-mm size was used for calculating the MEG gain (i.e., lead-field) matrix, which leads to a grid with $\sim$10,000 nodes covering the whole brain. MRIs were reviewed by a board-certified neuroradiologist (JRH), who determined that no mTBI or healthy control participant had visible lesions on MRI.

MEG source magnitude imaging using Fast-VESTAL

Voxel-wise MEG source magnitude images were obtained using our high-resolution Fast Vector-based Spatio-Temporal Analysis (Fast-VESTAL) MEG source magnitude imaging method.[67,88] This approach requires the sensor waveform covariance matrix. The artifact-free, eyes-closed, rs-MEG sensor-waveform datasets were divided into 2.5-sec sections. The data in each section were first direct current (DC)-corrected and then run through one of the following band-pass filters for delta (1-4 Hz) and gamma (30-80 Hz) bands. Notch filter at 60 Hz was applied to remove the power line signals.

Waveforms from all 306 sensors were used in the analysis. Sensor-waveform covariance matrices were calculated in the time domain for individual sections after the band-pass filtering, in the same way as in our previous studies to preserve the phase information.[54,88] Then the final sensor-waveform covariance matrix was obtained by averaging the covariance matrices across individual sections for the concatenated 10-min rs-MEG data that combined the two 5-min blocks. From the covariance matrix, whole-brain MEG source magnitude images for each frequency band were obtained for each participant using the Fast-VESTAL procedure.[67,88,89]

Design of rs-MEG machine learning approach

The proposed rs-MEG ML approach is a supervised leaning method. Figure 1 shows the diagrams of the ML approach. In the 98 participants and for each frequency-band model, voxel-wise whole-brain rs-MEG source images obtained from Fast-VESTAL were first spatially registered to the Montreal Neurological Institute (MNI)-152[90] brain-atlas template using FLIRT, an affine transformation program from FSL software.[91,92]

Spatial convolution and Max-pooling using functional regions of interest (ROIs). Once in MNI-152 space, the rs-MEG source imaging data from all frequency bands were first run through a spatial convolution layer. This convolution operation convolved the imaging data with a 3D Gaussian kernel with 5.0 mm full width half maximum (FWHM) to further reduce the inter-subject variability in anatomy. Then, a Max-pooling procedure was applied to the spatially convolved rs-MEG source imaging data. In this procedure, the MEG source imaging voxels were grouped into 184 gray matter functional ROI variables using the FCONN parcellation with similar sizes.[93] In each functional ROI, the maximum activity was obtained across all voxels within such an ROI. After regressing out age, 184 ROI features for each frequency band were obtained

The spatial convolution and Max-pooling procedure based on functional ROI played important roles in feature selection and dimension reduction, which is similar to the steps in 3D Convolutional Neural Networks (3D-CNN) for imaging processing,[94] except for two main differences. The first main difference is spatial convolution uses only the Gaussian kernel in rs-MEG ML, without any spatial-gradient based convolutional filters. The second main difference is that the Max-pooling is based on functional ROI in rs-MEG ML, rather than on Euclidean distance in 3D-CNN. These differences are discussed below.

Only one convolutional filter with Gaussian smoothing kernel was used in rs-MEG ML. This is one main difference between rs-MEG ML and the typical CNN approaches that use a large number of spatial gradient-based convolutional

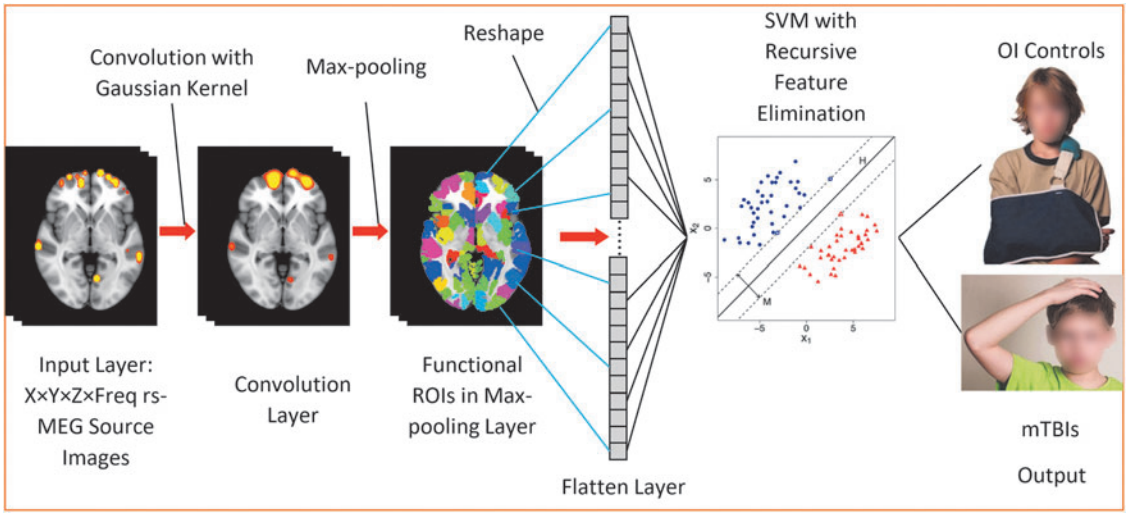

FIG. 1. Support vector machine (SVM) machine-learning diagram. The input images include resting-state magnetoencephalography (rs-MEG) source imaging volumes in standard Montreal Neurological Institute (MNI)-152 space across different frequency bands and participants. The rs-MEG source images are first convolved with a Gaussian kernel. Next, the maximum values from individual functional regions of interest are pooled to form the Pooling Layer. The elements in the Pooling Later are reshaped into the Flatten Layer. SVM with Recursive Feature Elimination is used to classify the individuals into either orthopedic injury (OI) or mild traumatic brain injury (mTBI) groups.

filters for processing structural images.[95–100] The gradient-based convolutional filters are good for detecting edges and shapes in images, and they usually require a large number (e.g., thousands) of samples to train. However, rs-MEG source magnitude images only contain ''hot spots'' without edge, shape, and other features. The single layer of convolutional filter with a Gaussian smoothing kernel in rs-MEG ML, in combination with our Max-pooling layer (see below) using 184 functional ROIs, effectively achieved the goal of dimension reduction using a smaller number of samples to train.

The Max-pooling procedure based on functional ROIs[93] was used in rs-MEG ML, instead of the geometric Max-pooling procedure based on Euclidean distance in typical CNN.[95–100] It is common that functionally distinct regions are next to each other with small Euclidean distance. The functional ROI-based Max-pooling has the advantage of taking into consideration the boundaries of functionally distinct regions. The rs-MEG source activity from the variables were reshaped into a 1-dimensional Flatten Layer for: 1) classifying mTBI and OI participants; and 2) predicting the symptom recovery in terms of PCS with a regression model. Age was projected out before further analyses.

Use rs-MEG ML to classify mTBI and OI participants. For a training data set, SVM-classification function with Recursive Feature Elimination (RFE)[101-103] was used to obtain the optimal ROI features from the Max-pooling ROI variables across all frequency bands (Fig. 1). Initially, all K variables present in our ROI dataset were included in training the network model. Then, the performance of the RFE-SVM model was calculated. Next, we computed the performance of the model after eliminating each variable (K times). Specifically, we dropped one ROI variable every time and trained the model on the remaining K-1 variables. The ROI variable whose removal had produced the smallest (or no) change in the performance of the model was dropped. This process was repeated until no ROI variable could be eliminated. The source activity from the subset of ROI variables after the RFE were sent to SVM classification. In the SVM classification model (Fig. 1), ''H'' stands for hyperplane(s) and ''M'' stands for maximum margin(s). The specific functions of SVM classification and RFE will be from the Scikit-lean Python Package. The output classes as shown in Figure 1 were the mTBI and OI groups

The performances of rs-MEG ML were examined for each individual frequency band, by changing the rs-MEG source imaging data in the Input Layer from the combined both-frequency bands data to that from each frequency band. The rest of the network design remained the same.

Use rs-MEG ML to predict PCS recovery with regression. Additionally, we examined the ability of the rs-MEG ML approach for predicting the recovery with respect to PCS.

In this approach, the ML diagram was similar to Figure 1, except the SVM-regression function was used for predicting the PCS scores and replaced the SVM-classification function. The rs-MEG data at the acute/sub-acute injury visit was used to predict the PCS score changes between the 3-month follow-up visit and the acute/sub-acute visit (i.e., 3-month PCS score minus the acute/sub-acute PCS score)

Model building and performance evaluation for rs-MEG classification

The present rs-MEG ML model was built using a supervised learning approach. The entire set of 98 participants (59 mTBI and 39 OI) was used to generate the predictive model. The model performance was evaluated using Monte Carlo cross-validation.[104] The participants were randomly split into a training set of 88 individuals (89.8%) and a validation set of 10 individuals (10.2%). The training set was used to establish the rs-MEG ML model, with the prediction accuracy computed on the validation set. The procedure was repeated 1000 times, with model performance averaged over the 1000 iterations. To control for label imbalance, the proportion of OI participants in each validation set was constrained to 30-70%. Age was projected out from the rs-MEG data before the above analyses were conducted.

The evaluation of model performance included: 1) sensitivity = TP/P, where P is number of mTBI subjects in the validation set and TP is the number among these correctly labeled as mTBI by the model; and 2) specificity = TN/N, where N is number of OI subjects in the validation set and TN is the number among these correctly classified as OI. SVM is a forced classification approach: it does not output individual-level classification probabilities, so no classification thresholds were used in determining sensitivity and specificity (e.g., via receiver operating characteristic [ROC] curves). Note that due to the limited sample size, the classification procedure uses the entire dataset for model training, with model evaluation via cross-validation, rather than splitting it into a training and testing dataset.[105] Monte-Carlo cross-validation was found in standard settings to more accurately estimate predictive performance than other options such as leave-one-out cross-validation.[106,107] The choice of a 90:10 split of the training:validation sample in cross-validation corresponds to the choice of K = 10 for K-fold cross-validation, which is recommended as finding a balance between accurate estimation of predictive performance and leaving enough data for model training.[105]

Conventional voxel-wise analyses for rs-MEG source imaging

Additional analyses were conducted using the conventional MEG source magnitude imaging using a voxel-wise statistical analysis approach.[67] In this approach, the registered rs-MEG source magnitude images in MNI-152 space were spatially smoothed using a Gaussian kernel with 5 mm FWHM, followed by a logarithmic transformation using FSL. Then, a voxel-wise, analysis of covariance (ANCOVA) was performed to test for differences between the mTBI and control groups, with age as a covariate. Family-wise error rate across voxels were controlled by using a standard cluster analysis for the t-value maps to create the corrected group statistical maps ($p < 0.01$) for the MEG source magnitude images.[67]

Training and testing procedure for rs-MEG to predict PCS recovery

To predict PCS recovery (i.e., difference score, 3-month PCS score minus the acute/sub-acute PCS score) using the ML with rs-MEG data collected during the acute/sub-acute exam, the mTBI and OI groups were analyzed separately. For the mTBI group, the training data set contained 53 (or 89.8%) children and the testing data set contained six (or 10.2%) children. Again, to examine the robustness of the performances of rs-MEG ML, the procedures were repeated for 1000 different combinations of the 53 – 6 splits. For the OI group, the number of children in the training and validation data sets were 35 (or 89.7%) and four (or 10.3%), respectively. The procedures were repeated for 1000 different combinations of the 35 – 4 splits.

We focused on the combined rs-MEG ML model with both delta- and gamma-activity. Age was projected out from both the rs-MEG and the PCS difference score before these analyses were conducted. Two measures were used to assess the predictive performance of the rs-MEG ML approach: 1) the correlation value across subjects between the measured and ML-predicted PCS scores, and 2) the variance explained on the testing data sets by the ML-predicted PCS score out of the measured PCS score.

Results

Table 1 details demographic and clinical characteristics of the participants. The mTBI and OI groups consisted of 59 and 39 participants, respectively. Despite efforts to match the groups by age, mean (standard deviation [SD]) age at baseline assessment was significantly higher for the mTBI group versus the OI group [12.05 (SD = 2.22) versus 11.18 (SD = 1.88); t = 2.02; df = 96; $p = 0.046$]. Therefore, the MEG ML analyses controlled for age. In terms of GCS, the mTBI group had one participant with a GCS score of 13, two participants with a GCS score of 14, and 56 participants with a GCS score of 15, whereas in the OI group, by default, all 39 participants had a GCS score of 15. The study neuroradiologist, JRH, detected trauma-related abnormalities in 5/59

Table 1. Demographic and Clinical Characteristics

	mTBI (n = *59*)		*OI* (n = *39*)				
	Mean	*SD*	*Mean*	*SD*	*t*	*df*	p *value*
Age at baseline	12.05	2.22	11.18	1.88	2.02	96	0.046
Glasgow Coma Scale Score	14.932	0.314	15	0	-1.66	58	0.103
WASI-II Full Scale IQ	107.64	12.15	109.03	14.67	-0.49	70.73	0.627
Days between injury and baseline	24.29	6.68	21.69	5.88	1.97	96	0.051
Days between injury and MRI	52.80	21.70	48.56	23.90	0.91	96	0.366
Days between baseline and follow-op	82.42	15.27	86.15	14.60	-1.20	96	0.231
Days between injury and follow-up	106.24	13.92	107.59	14.25	-0.47	96	0.642
Parent HBI—1 month prior to injury							
Cognitive	8.47	7.23	6.13	6.45	1.64	96	0.208
Somatic	1.58	2.44	1.08	2.60	0.97	96	0.672
Total	10.05	8.51	7.21	7.52	1.70	96	0.093
Parent HBI—baseline (acute/sub-acute visit)							
Cognitive	9.51	8.20	5.72	6.45	2.55	93.0	0.012
Somatic	4.98	6.12	1.36	2.60	4.03	84.4	0.000
Total	14.49	12.67	7.08	7.66	3.61	95.4	0.000
Parent HBI - 3-month follow-up							
Cognitive	8.12	7.25	6.59	6.09	1.09	96	0.558
Somatic	2.53	3.97	1.13	2.44	2.16	95.6	0.066
Total	10.64	9.51	7.72	7.18	1.73	94.2	0.087
Parent HBI—3-month follow-up minus baseline (acute/sub-acute visit) difference scores							
Total difference	-3.85	10.04	0.64	6.26	-2.725	95.7	0.008

The p values for the Cognitive and the Somatic domains reflect two-fold Bonferonni correction.

mTBI, mild traumatic brain injury; OI, orthopedic injury; SD, standard deviation; HBI, Health and Behavior Inventory Scale; WASI II, Wechsler Abbreviated Scale of Intelligence-Second Edition; MRI, magnetic resonance imaging.

(8.5%) of the research MRI scans in the mTBI group. The mTBI and OI groups were predominantly male (39/59 [66.1%] and 25/39 [64.1%]), respectively (Fisher's exact test p = 1.00). Right handedness in the mTBI and OI groups was present in 56/59 (94.9%) and 34/39 (87.2%), respectively (Fisher's exact test $p = 0.26$). The groups did not significantly differ on global intellectual functioning as measured by the Wechsler Abbreviated Scale of Intelligence-Second Edition (WASI-II)[108] Full Scale IQ-2 subtest score (mTBI mean = 107.64, SD = 12.15, OI mean = 109.03, SD = 14.67; t = -0.49; $p = 0.627$).

Participants attended three research sessions at different time-points: 1) at baseline (days between injury and baseline for mTBI group mean = 24.29, SD = 6.68, for OI group mean = 21.69, SD = 5.88; t = 1.97; df = 96; $p = 0.051$), 2) at MRI (days between injury and MRI for mTBI group mean = 52.80, SD = 21.70, for OI group mean = 48.56, SD = 23.90; t = 0.91; df = 96; $p = 0.366$), and 3) at 3-month follow-up (days between baseline and follow-up for mTBI group mean = 82.42, SD = 15.27, for OI group mean = 86.15, SD = 14.60; t = -1.20; df = 96; $p = 0.231$).

The Parent HBI scores at the three assessment time-points are tabulated in Table 1, and group (mTBI vs. OI) comparisons were analyzed with independent sample t-tests. Parent HBI symptom rating total scores for the mTBI group ranged from 0 to 51 at baseline acute/sub-acute visit (average approximately 3 weeks post-injury) and 0 to 38 at the 3-month follow-up. Parent HBI symptom rating total scores for the OI group ranged from 0 to 28 at baseline acute/sub-acute visit and 0 to 29 at the 3-month follow-up. The difference scores for parent HBI symptom rating total scores at 3-month follow-up minus baseline acute/sub-acute visit ranged from -34 to 18 for the mTBI group, and -17 to 16 for the OI group. The baseline acute/sub-acute visit parent HBI symptom rating total for mTBI participants (mean = 14.49, SD = 12.67) was significantly higher than the comparison group (mean = 7.08, SD = 7.66); t = 3.61; df = 95.4; $p = 0.001$). The component domain scores were: cognitive score for mTBI (mean = 9.51, SD = 8.20) versus OI (mean = 5.72, SD = 6.45); t = 2.55; df = 93; $p = 0.025$ and somatic score for mTBI (mean = 4.98, SD = 6.12) versus OI (mean = 1.36, SD = 2.60); t = 4.03; df = 84.4; $p = 0.001$, both Bonferroni-corrected.

Although parent HBI symptom ratings from the 1-month prior to injury and from the 3-month follow-up were higher for the mTBI as compared with the OI group, differences did not survive Bonferroni-correction (Table 1).

The parent HBI ratings difference total score from the 3-month follow-up minus the baseline acute/sub-acute visit was significant across groups. Negative values in difference total scores indicate improvement in symptoms and positive values in difference total scores indicates worsening in symptoms. The mTBI group showed a higher difference in total scores with mean = -3.85, SD = 10.04 versus the OI group's mean = 0.64, SD = 6.26; t = -2.725; df = 95.7, $p = 0.008$.

Classification accuracy of mTBI versus OI, and ROC analyses of rs-MEG ML

The classification accuracies of rs-MEG ML in the validation sets are shown in upper panel of Table 2 and Figure 2 for each model. Fast-VESTAL source magnitude imaging data were used as the input layer. The ML approach integrated rs-MEG source imaging markers across delta-band and gamma-band frequencies. The left panel of Figure 2 shows the classification accuracies in testing data sets from the mTBI and OI control groups, plotted for combined delta-gamma, delta only, and gamma only bands. The accuracies in the mTBI group (i.e., sensitivity measures) were $95.5 \pm 1.6\%$, $89.6 \pm 2.6\%$, and $85.2 \pm 3.2\%$, for the combined delta-gamma, delta only, and gamma only frequencies, respectively. The accuracies in the OI group (i.e., specificity measures) were $90.2 \pm 2.7\%$, $84.0 \pm 4.7\%$, and $78.3 \pm 3.7\%$, for the combined delta-gamma, delta only, and gamma only frequencies, respectively. Classification accuracies for the combined delta-gamma model were markedly better than for models using individual frequency bands (non-parametric Wilcoxon signed-rank test with paired samples: $p < 0.0001$). Figure 2 graphs the classification accuracies of the individual frequency band models for rs-MEG input.

The ROC analyses evaluated the overall accuracy of models by analyzing the area under the curve (AUC) for the sensitivity and specificity distributions using import ''roc_curve'', ''auc'' functions in Python's sklearn (version 1.0.2) package. The right panel of Figure 2 shows the ROC curves for the three models. All curves markedly outperformed the naive/non-discretionary classifier (diagonal dashed line). However, the combined delta-gamma band model (blue curve) showed excellent performance with both high sensitivity and high specificity. The AUC value of the ROC was 98.5% for the combined delta-gamma model. This value was significantly higher than delta-only model (AUC: 92.6%) or gamma-only model (AUC: 89.6%) using Wilcoxon signed-rank test with paired samples ($p < 0.001$).

Table 2. Results of rs-MEG ML Analysis, the Categorical Classification Accuracies (Sensitivity and Specificity) and the Area Under the Curve (AUC) of the Receiver Operating Characteristic (ROC) Curve in Testing Data Sets for Delta Plus Gamma (bold), Delta-Only, and Gamma-Only Band Models

rs-MEG ML Model	*$\delta + \gamma$ bands (%)*	*δ band only (%)*	*γ band only (%)*
59 mTBI (sensitivity)	**96.9 ± 1.9**	87.2 ± 2.9	83.5 ± 3.1
39 OI (specificity)	**90.1 ± 3.1**	82.5 ± 4.5	78.4 ± 3.8
AUC of ROC (%)	**98.5**	92.6	89.6
95% CI for AUC	**96.7 to 99.6**	89.5 to 95.3	86.7 to 92.9

rs-MEG ML, resting-state magnetoencephalography; mTBI, mild traumatic brain injury; OI, orthopedic injury; CI, confidence interval.

Predict PCS recovery using ML and acute/sub-acute rs-MEG

The prognostic value of ML approach on the validation data sets was studied using the rs-MEG data collected during the acute/sub-acute exam to predict the recovery of PCS at 3-month follow-up. Here, the SVM ML method with the combined delta-gamma band rs-MEG signals in the acute/sub-acute exam was used to predict later changes in PCS (3-month minus 3-week) in children with mTBI ($N = 59$). Figure 3 shows the measured parent-rated symptom score changes and the predicted symptom score changes by ML were highly correlated. Each color column represents an individual child, and the spreading resulted from the 1000 bootstrapping analysis. On the testing data sets, the correlation value across subjects between the measured and predicted PCS scores was 0.903, and the variance explained by the predicted model was 84.5% with mean squared error (MSE) of 17.7, suggesting that acute/sub-acute rs-MEG using ML could accurately predict the PCS recovery in children with mTBI. In contrast, for the OI group ($N = 39$, not shown), the corresponding correlation, variance explained, and MSE by deep learning model were 0.762, 65.6%, and 13.3, respectively. These values were significantly lower than those in the mTBI group (Mann-Whitney test, $p < 10^{-4}$).

Spatial differences in rs-MEG activity using voxel-wise analyses

Conventional voxel-wise ANCOVA was used to assess spatial differences in rs-MEG activity with age as a covariate. Compared with children with OI, Figure 4 shows that children with mTBI showed abnormal increases in delta-band activity from the frontal poles, rostral anterior cingulate cortex (rACC), superior central areas, posterior insular, parietal operculum cortex, lateral temporal lobe, precuneous cortex, lingual cortex, and basal ganglia. The mTBI group also showed mainly abnormal increases in gamma-band activity from frontal poles, inferior frontal gyrus, planum temporale in lateral temporal lobe, superior central areas, hippocampus, fusiform gyrus, and cerebellum, but decreases from medial frontal cortices, inferior temporal gyrus, and lateral occipital cortex.

Associations between rs-MEG regional activity and PCS recovery

Figure 5 displays scatter plots in which changes in PCS score (3-month minus 3-week, unscaled) were plotted against two hypothesized regional rs-MEG markers derived from ML algorithm: right and left frontal pole (FP) areas in gamma band. Figure 5 shows that in 59 children with mTBI (but not in 39 children with OI), the rs-MEG activity positively correlated with changes in PCS. In these two regions, the children with mTBI also showed abnormal hyper-activity in gamma band rs-MEG (see

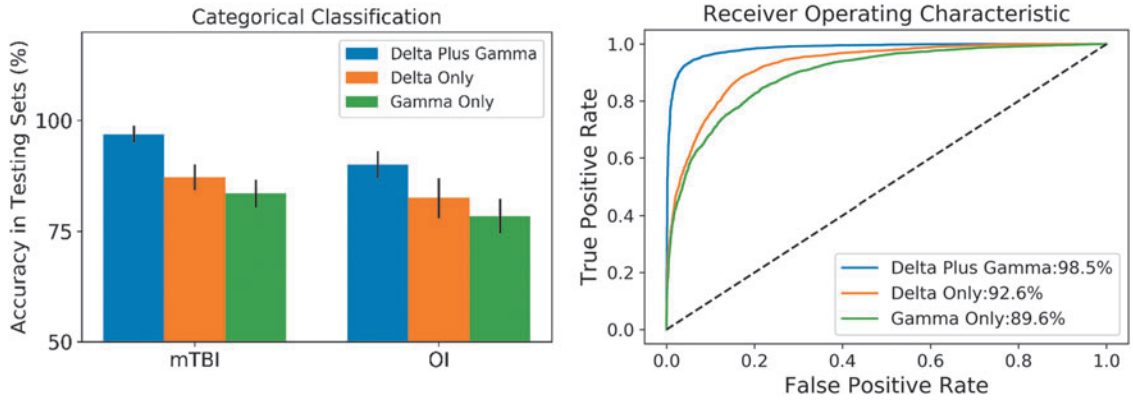

FIG. 2. Machine learning's classification accuracy in children with mild traumatic brain injury (mTBI) and orthopedic injury (OI) controls using resting-state magnetoencephalography (rs-MEG) signals from delta, gamma, and combined delta-gamma bands. Left panel: classification accuracy; right panel: receiver operating characteristic (ROC) curves. The % values in the figure are area under the curve (AUC) values. The AUC value for the combined delta-gamma model was significantly higher than those using the delta or gamma only band.

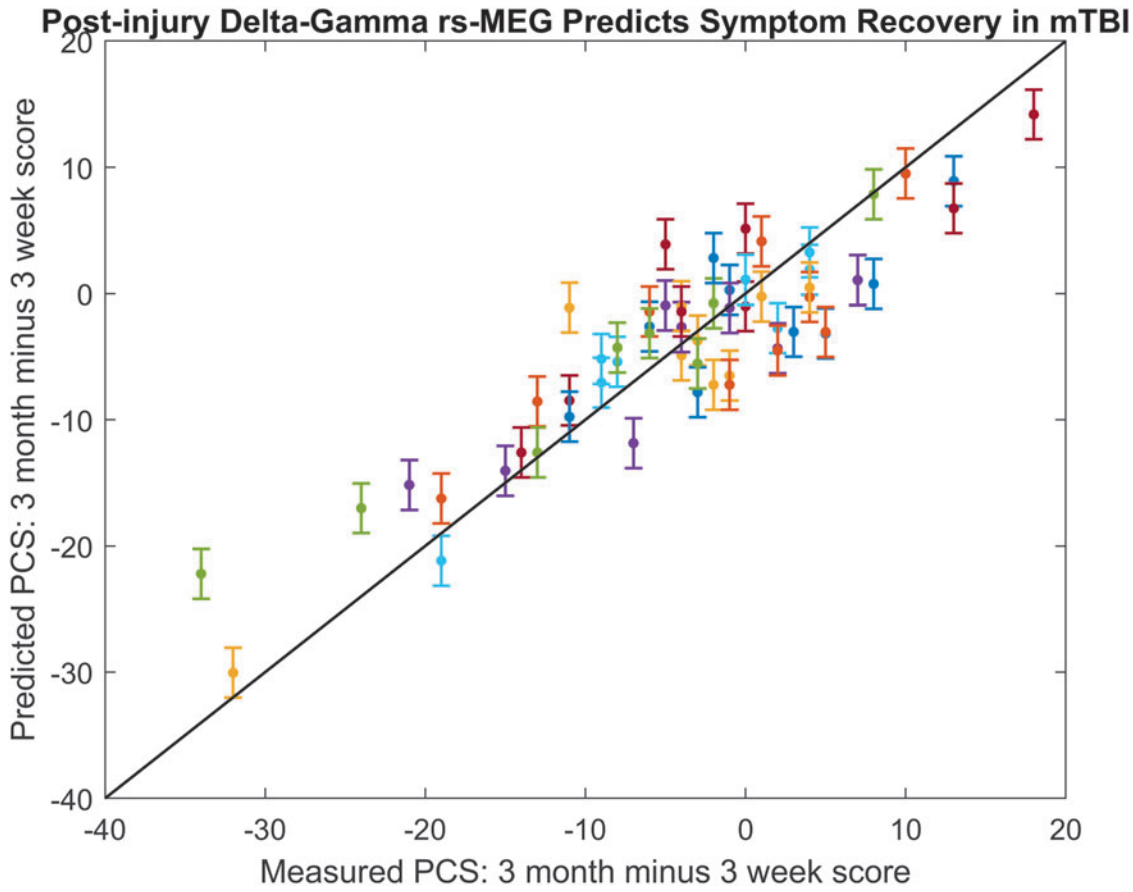

FIG. 3. Delta plus gamma band model used resting-state magnetoencephalography (rs-MEG) in 3-week acute/sub-acute post-injury examination to predict 3-month recovery in terms of post-concussive symptoms in $N = 59$ children with mild traumatic brain injury (mTBI). The mean values across 1000 bootstrapping and 95% confidence intervals were plotted for each subject.

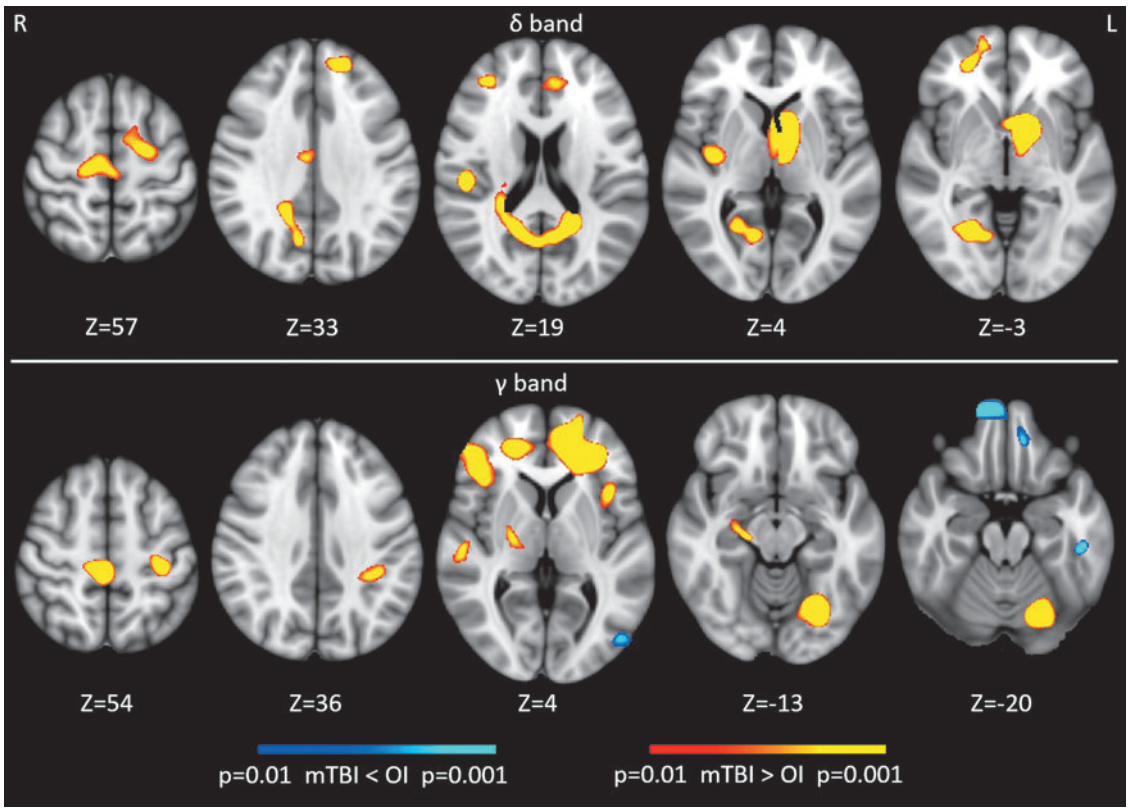

FIG. 4. Voxel-wise resting-state magnetoencephalography activity from delta and gamma frequency bands in pediatric mild traumatic brain injury (mTBI) versus orthopedic injury (OI). The values in Z are superior-inferior coordinates of the axial slices in the Montreal Neurological Institute (MNI) space.

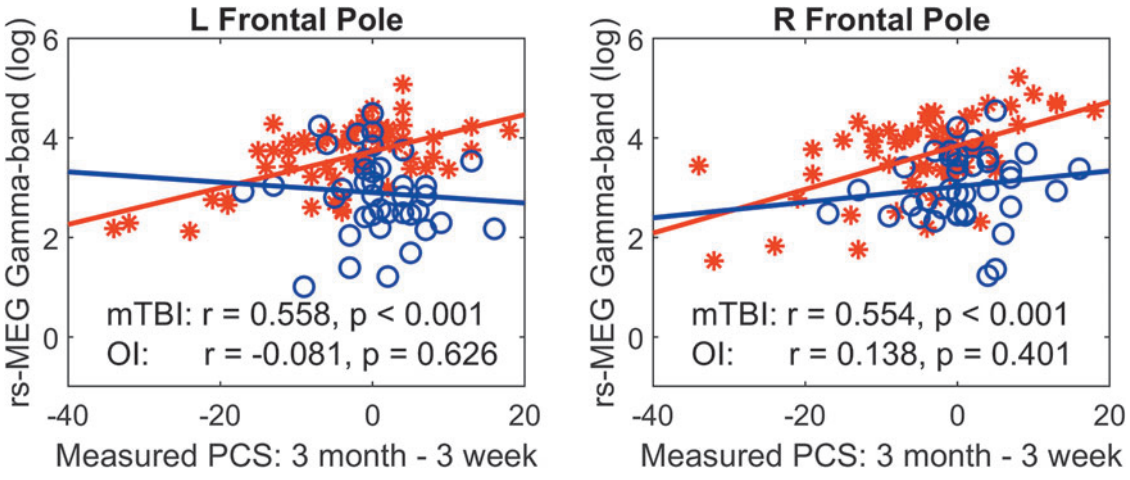

FIG. 5. Scatter for left and right frontal poles plots between resting-state magnetoencephalography (rs-MEG) markers in gamma band and post-concussive symptom recovery. Red stars: children with mild traumatic brain injury (mTBI); blue circles: children with orthopedic injury (OI).

y-axis). These show that increases in gamma activity from FP areas predict poor symptom outcomes only in children with mTBI but not with OI.

Discussion

There were four main findings in this rs-MEG study of children with mTBI as compared with children with OI. The first two findings provided answers for the initial overarching question regarding a neural injury signature of pediatric mTBI. The second two findings presented answers for the second overarching question about the pattern(s) of neural injury that determine behavioral recovery from early post-injury to sub-acute outcome at 3-month post-injury.

First, the ML algorithm predicted cases of mTBI versus OI with sensitivity and specificity both over 90% ($95.5 \pm 1.6\%$ and $90.2 \pm 2.7\%$, respectively) at 3-weeks post-injury for the combined delta-gamma frequencies (Fig. 2; Table 2). Further, the sensitivity and specificity metrics were significantly better for the combined delta-gamma frequencies compared with the delta-only and gamma-only frequencies. These findings supported hypothesis 1a. Second, the analyses found spatial differences in rs-MEG activity between mTBI and OI groups in both delta and gamma bands in frontal and temporal lobes as hypothesized (hypothesis 1b), but also more widely in the brain (Fig. 4). Third, the ML algorithm with post-injury rs-MEG data accounted for 84.5% of the variance in predicting recovery as measured by PCS changes between 3 weeks post-injury and the 3-month outcome in the mTBI group (Fig. 3), and this metric was significantly lower in the OI group (65.6%, $p < 10^{-4}$). This is the first example of rs-MEG predicting behavioral recovery in a prospective longitudinal study of either children or adults. These results supported hypothesis 2.

Fourth, scatter plots (Fig. 5) displayed two hypothesized regional (right and left frontal pole) rs-MEG gamma band markers derived from the ML algorithm that illustrated (higher) gamma band activity significantly associated with (worse) PCS outcome at the 3-month PCS assessment compared with the 3-week assessment exclusively in the pediatric mTBI group. This fourth finding offers an important example regarding regional specifics undergirding the ML algorithm predicting recovery at 3-months post-injury and is a step toward developing a model for pattern(s) of neural injury that determine behavioral outcome.

The findings that involve delta and gamma band are consistent with adult mTBI studies and therefore build upon our preliminary work[50] in extending these functional imaging findings to a pediatric mTBI cohort. For example, regional rs-MEG slow-wave markers are detected in the acute, sub-acute, and chronic phase of adult mTBI,[57] and are also sensitive in differentiating chronic and sub-acute patients with adult mTBI who have persistent PCS from neurologically normal individuals.[55,56,62,65,66] Further, adults with combat-related mTBI show significant hyperactivity in rs-MEG gamma band markers.[67]

The findings in this rs-MEG study underscore that the neuropathophysiology in the sub-acute (3 weeks post-injury) phase after pediatric mTBI intimately involves GM alteration. Neuroimaging research related to pediatric mTBI has focused on white matter network changes from DAI.[16,22–42] It is well-accepted that acceleration-deceleration forces that act at the time of the mTBI may lead to DAI.[109] GM damage has been more difficult to detect than DAI unless there are macroscopic cortical contusions, which are rare after pediatric mTBI. Decreased GM and white matter integrity are related to action of dynamic forces to the brain unique to each mTBI. These forces precipitate initial ionic fluxes, and indiscriminate glutamate and metabolic coupling that cause oxidative stress, impaired axonal transportation, and altered neurotransmission.[110] rs-MEG studies offer a path towards a detailed neurophysiological mechanistic understanding of the clinical implications specifically of GM dysfunction consistently characterized by abnormal delta and gamma bands in children and adults with mTBI.

It appears that the abnormal delta and gamma signals are related to different mechanisms. Neurophysiological studies in animals have established a solid connection between pathological delta-wave (1-4 Hz) generation in GM and injuries. Delta-band activity produced by physical lesions in cats were localized to the GM of cortex overlying the lesion.[111,112] Abnormal delta-waves can also be induced by the administration of atropine.[113] Atropine is a competitive antagonist of acetylcholine (ACh) receptors and can block and/or limit ACh. These animal experiments concluded that cortical deafferentation was a key factor in abnormal delta-wave production, owing to DAI and/or blockages/limitations in the cholinergic pathway.[114]

A postulated mechanism of hyperactivity of gamma band finding is as follows. DAI plays a major role in brain dysfunction producing an imbalance in excitatory/inhibitory neural activity after mTBI. In GM, DAI is also directly associated with injuries to GABA-ergic inhibitory interneurons, specifically the parvalbumin-positive (PV+) interneurons.[61] In addition, DAI in GM is perisomatic, near the soma of the PV+ interneurons,[61] or with a degradation of the perineuronal net (PNN), a specialized extracellular structure enwrapping cortical PV+ inhibitory interneurons.[115] Fast-spiking (FS) PV+ inhibitory interneurons are the most common type of GABA-ergic cells that regulate the activity of neural networks through GABA-ergic inhibition of local excitatory neurons, and synchronous activity of FS-PV+ interneurons generates gamma oscillations (30-80 Hz).[116–120] Animal studies demonstrate that dysfunction or injury

to PV+ interneurons causes disinhibition in the neural network, directly eliminating synchronized gamma-band (30-80 Hz) signals that are normally evoked by stimuli,[116,121,122] and up-regulating spontaneous gamma activity (and possibly beta activity), owing to a lack of inhibition of pyramidal and other excitatory neurons.[116,121–124]

With the growing recognition of the importance of GM integrity after mTBI, particularly in adult MEG research, and now in pediatric mTBI, the next steps are to refine our understanding of the pathophysiology of injury and recovery. There are several approaches that are likely to be fruitful. First, prospective longitudinal studies such as the current study will be more convincing than cross-sectional or retrospective studies. Second, examination of different rs-MEG bands or combined bands should be more useful than single bands as shown in the current study.[125] More in-depth understanding of the function of each of the band frequencies in injured and uninjured populations will be important. In the current study, we focused on delta and gamma bands, but our preliminary data demonstrated significant differences in alpha and beta bands between participants with mTBI and OI.[50] The main reason we focused on delta and gamma bands was because the models that used these bands outperformed those using alpha or beta bands, as shown in a separate mTBI study with machine learning.[126] Third, larger controlled studies will have more power to detect important findings including those that involve other bands. The reasons for the increase in power includes the fact that while every injury is unique, the larger the cohort, the more likely one would detect common patterns of injury and recovery.

Fourth, larger rs-MEG studies would permit a biopsychosocial analytic approach that includes psychosocial factors, which we and others have shown to be relevant to behavioral and psychiatric outcome after mTBI.[5,6,12,13] Fifth, ML techniques have demonstrated power to detect meaningful analyses of neural signatures of injury as well as pattern(s) of neural injury that determine behavioral recovery. Deep learning techniques may be even more powerful and mitigate the need for very large cohorts. Sixth, integration of rs-MEG findings with GM diffusion techniques as well as white matter microstructural studies might deepen understanding of neural signatures of injury and patterns of neural injury that determine behavioral recovery. Seventh, standardized clinician-rated psychiatric interviews that elicit symptoms and/or disorders, and which integrate the clinician's observation of the child, as well as the respective symptom reports of both parent and child are considered the gold-standard for behavioral assessment, and should improve study methodology.

Compared with our previous pilot study with a smaller cohort,[50] the results of voxel-wise analyses with a much larger cohort from the present study revealed additional brain regions of significant group difference for both the delta and gamma bands. For the low frequency delta band, we replicated our earlier finding of increased activity in the lateral temporal lobe using the larger cohort in the present study. Additionally, we found regions of significant difference in frontal poles, rACC, superior central areas, posterior insular, parietal operculum cortex, precuneus cortex, lingual cortex, and basal ganglia in the larger cohort as opposed to our preliminary work in the smaller cohort. For the gamma band, the finding of increased activity in the cerebellum was consistent in both cohorts. However, in the present study, mTBI group also showed abnormal increases in gamma-band activity from frontal poles, inferior frontal gyrus, planum temporale in lateral temporal lobe, superior central areas, hippocampus, fusiform gyrus, and cerebellum, but decreases from medial frontal cortices, inferior temporal gyrus, and lateral occipital cortex. The gamma-band activity from these regions did not show significant group differences in the pilot study. The new significant findings from the present study are likely due to increased power from the larger sample size. Note that the subjects studied in the pilot study were not used in the present study due to the MEG being conducted at different points of recovery (i.e., 6 months post-injury in the pilot study vs. 3 weeks post-injury in the present study).

The 90% thresholds for both sensitivity and specificity adopted by our study are very high standards demonstrating the rigor of our approach and the performance of the proposed algorithm. The $R^2 = 80\%$ for predicting recovery of PCS symptoms is also a high threshold, although general guidelines are not available in this setting.

Different from the current rs-MEG study that utilizes voxel-wise source magnitude, voxel-wise functional connectivity (FC) using rs-MEG or rs-fMRI is another approach for studying mTBI. However, as reviewed in our previous study,[54] increase, decrease, or concurrent increase and decrease in FC have all been reported rs-fMRI and rs-MEG mTBI studies in adults. This may be due to the co-existence of multiple mechanisms at play during mTBI recovery.[54] First, mTBI may injure white matter (WM) tracts, resulting in the disruption of neuronal communication between gray matter (GM) areas, which may lead to decreased FC with other brain regions, especially if axonal damage is substantial. An alternative is glutamate-based over-excitation and GABAergic disinhibition, another leading mechanism for mTBI-related secondary injury, which involves compromise to neurons in the GM. The glutamate over-excitation and GABA disinhibition model posits aberrant GABA intra-neuron functioning, which diminishes the inhibitory influence on pyramidal neurons, thereby causing increased firing and facilitation of network connections that are normally inhibited. This process could lead to increases in FC between the injured GM area and other regions of the brain.

A third potential mechanism that may also contribute to increases in FC is the functional reorganization model, which involves compensation or rerouting of functional connections after mTBI.

Our findings are generally consistent with other reports of functional imaging alterations in both adults and children with mild to moderate TBI, which reflect increases in neural connectivity, particularly in the frontal lobes, potentially implicating compensatory recruitment of additional brain regions, inefficiency, a failure in decoupling anterior brain regions in effortful processing, or alteration of typical development in connectivity patterns.[127–132] Studies using graph theory in children with mTBI have also revealed altered network organization in relation to trauma comparison groups as reflected by lower modularity, higher small-worldness, and lower assortativity,[133] which in turn relate to poorer cognitive and behavioral outcome.

The study had several limitations foreshadowed in the above discussion of likely fruitful future approaches. First, the rs-MEG analyses were limited to gamma and delta bands. Examination of other bands including alpha, beta, and theta bands, and combinations of these bands would provide a more complete picture of the neural signature of pediatric mTBI and patterns of neural injury related to recovery. Second, the relatively modest sample size resulted in insufficient power to detect important findings including those related to other bands. However, the sample size was relatively large for this type of functional imaging research, especially MEG studies. Third, the limited power related to the sample size precluded analyses that control for potentially confounding psychosocial variables that have been shown to be related to behavioral outcome after pediatric mTBI.[6] Fourth, our ML approach was not as powerful as a deep learning approach. Fifth, we have not integrated the rs-MEG findings with white matter microstructural data or with GM diffusion data, which could provide a more fundamental understanding of neural signatures of injury and patterns of neural injury related to behavioral recovery.

Sixth, only parent-rated PCS scores were analyzed. Child self-report PCS ratings would likely provide a different pattern of results, which might provide an alternative understanding of brain-behavior relationships. Seventh, the validity and reliability of the concept of PCS itself has been questioned.[134] Clinician-rated psychiatric symptoms and/or disorders would likely provide a superior behavioral assessment.[52] Eighth, there is a potential confound affecting MEG results with regard to comorbid psychiatric conditions. However, the research protocol standardized psychiatric assessment,[135] which was not a focus of these analyses showed approximately equivalent prevalence of pre-injury disorders in mTBI versus OI such as ADHD (mTBI 8/59 (13.6%); OI 4/39 (10.3%), anxiety disorders (mTBI 17/59 (28.8%); OI 8/39 (20.5%), and substance abuse (none in either group). Ninth, the OI group was significantly younger (by an average of 12 months) than the mTBI group. However, this was mitigated by controlling for age in the rs-MEG analyses.

There were several notable strengths of the study. First, this was a prospective longitudinal study of a non-selected series of consecutively treated patients with pediatric mTBI. As such, it was only the second such study and followed our preliminary study, which had a sample size of less than one quarter of the current study.[50] Second, the design included appropriate control participants who had similar IQ and sex representation, and presumably similar predisposing factors for incurring an injury and experience of trauma and treatment in the ED. Third, state-of-the-art rs-MEG techniques and analyses were used in the study.

There were several clinical implications of the study. The findings serve as a step toward understanding neural dysfunction after pediatric mTBI, which may have future clinical importance in the identification of groups of children who are at higher risk for incomplete or delayed recovery, or who are potentially at higher risk of recovery problems should they suffer an additional mTBI. An issue that has limited clinical application of MEG findings has been the cost and availability of this technology. MEG systems use Superconducting QUantum Interference Devices (SQUIDs) sensors.[136] However, Optically Pumped Magnetometers (OPMs) have emerged as a wearable alternative to SQUIDs. The laser-based OPM sensors do not require cryogenic cooling, and can be flexibly placed on any part of the body,[137,138] which permits less expensive, more flexible, and highly sensitive MEG systems.[139,140] Commercial MEG systems based on OPM are expected to be available soon, which will make MEG widely available for clinical and research applications including mTBI.

Authors' Contributions

Ming-Xiong Huang: Conception or design of the work; data analysis and interpretation; drafting the article; critical revision of the article; final approval of the version to be published.

Annemarie Angeles-Quinto: data collection; data analysis and interpretation; drafting the article; critical revision of the article; final approval of the version to be published.

Ashley Robb-Swan: Data collection; data analysis and interpretation; drafting the article; critical revision of the article; final approval of the version to be published.

Bianca G. De-la-Garza: Data collection; drafting the article; critical revision of the article; final approval of the version to be published.

Charles W. Huang: Data analysis and interpretation; drafting the article; critical revision of the article final approval of the version to be published.

Chung-Kuan Cheng: Data analysis and interpretation; drafting the article; critical revision of the article; final approval of the version to be published.

John R. Hesselink: Data analysis and interpretation; drafting the article; critical revision of the article; final approval of the version to be published.

Erin D. Bigler: Conception or design of the work; data analysis and interpretation; drafting the article; critical revision of the article; final approval of the version to be published.

Elisabeth A. Wilde: Conception or design of the work; data analysis and interpretation; drafting the article; critical revision of the article; final approval of the version to be published.

Florin Vaida: Conception or design of the work; data analysis and interpretation; drafting the article; critical revision of the article; final approval of the version to be published.

Emily A. Troyer: Data analysis and interpretation; drafting the article; critical revision of the article; final approval of the version to be published,

Jeffrey E. Max: Conception or design of the work; data analysis and interpretation; drafting the article; critical revision of the article; final approval of the version to be published.

Funding Information

This work was supported in part by 1R-01 HD088438-01A1 (PI: J.E. Max), and by Merit Review Grants from the Department of Veterans Affairs (PI: M.X. Huang, I01-CX000499, I01-RX001988, MHBA-010-14F, NURC-022-10F, NEUC-044-06S).

Author Disclosure Statement

Dr. Max provides expert testimony in cases of traumatic brain injury on an *ad hoc* basis for plaintiffs and defendants on a more or less equal ratio. This activity constitutes approximately 5% of Dr. Max's professional activity. Dr. Bigler provides expert testimony in cases of traumatic brain injury.

For the other authors, no competing financial interests exist.

References

1. Centers for Disease Control and Prevention: Report to Congress on the management of traumatic brain injury in children: opportunities for action. Atlanta, GA, USA; 2018. Available from: https://www.cdc.gov/traumaticbraininjury/pdf/reportstocongress/managementoftbiinchildren/TBI-ReporttoCongress-508.pdf [Last accessed March 4, 2023].
2. Taylor CA, Bell JM, Breiding MJ, et al. Traumatic brain injury-related emergency department visits, hospitalizations, and deaths—United States, 2007 and 2013. MMWR Surveill Summ 2017;66(9):1–16; doi: 10.15585/mmwr.ss6609a1
3. Faul M, Xu L, Wald MM, et al. Traumatic brain injury in the United States: emergency department visits, hospitalizations, and deaths. Atlanta, GA, USA; 2010. Available from: https://www.cdc.gov/traumaticbraininjury/pdf/blue_book.pdf [Last accessed March, 2023].
4. Cassidy JD, Carroll LJ, Peloso PM, et al. Incidence, risk factors and prevention of mild traumatic brain injury: results of the WHO Collaborating Centre Task Force on Mild Traumatic Brain Injury. J Rehabil Med 2004;43 Suppl):28–60; doi: 10.1080/16501960410023732
5. Yeates KO, Kaizar E, Rusin J, et al. Reliable change in postconcussive symptoms and its functional consequences among children with mild traumatic brain injury. Arch Pediatr Adolesc Med 2012;166(7):615–622; doi: 10.1001/archpediatrics.2011.1082
6. Max JE, Judd N, Bigler ED, et al. Three-month psychiatric outcome of pediatric mild traumatic brain injury: a controlled Study. J Neurotrauma 2021;38(23):3341–3351; doi: 10.1089/neu.2021.0324
7. Brown G, Chadwick O, Shaffer D, et al. A prospective study of children with head injuries: III. Psychiatric sequelae. Psychol Med 1981;11(1):63–78; doi: 10.1017/s0033291700053289
8. Luis CA, Mittenberg W. Mood and anxiety disorders following pediatric traumatic brain injury: a prospective study. J Clin Exp Neuropsychol 2002;24(3):270–279; doi: 10.1076/jcen.24.3.270.982
9. Max JE, Koele SL, Smith WL, Jr., et al. Psychiatric disorders in children and adolescents after severe traumatic brain injury: a controlled study. J Am Acad Child Adolesc Psychiatry 1998;37(8):832–840; doi: 10.1097/00004583-199808000-00013
10. Barlow KM, Crawford S, Brooks BL, et al. The incidence of postconcussion syndrome remains stable following mild traumatic brain injury in children. Pediatr Neurol 2015;53(6):491–497; doi: 10.1016/j.pediatrneurol.2015.04.011
11. Barlow KM, Crawford S, Stevenson A, et al. Epidemiology of postconcussion syndrome in pediatric mild traumatic brain injury. Pediatrics 2010;126(2):e374–e3781; doi: 10.1542/peds.2009-0925
12. Brooks BL, Plourde V, Beauchamp MH, et al. Predicting psychological distress after pediatric concussion. J Neurotrauma 2019;36(5):679–685; doi: 10.1089/neu.2018.5792
13. Max JE, Schachar RJ, Landis J, et al. Psychiatric disorders in children and adolescents in the first six months after mild traumatic brain injury. J Neuropsychiatry Clin Neurosci 2013;25(3):187–197; doi: 10.1176/appi.neuropsych.12010011
14. Engel GL. The biopsychosocial model and the education of health professionals. Ann N Y Acad Sci 1978;310:169–187; doi: 10.1016/0163-8343(79)90062-8
15. Ware AL, Goodrich-Hunsaker NJ, Lebel C, et al. Post-acute cortical thickness in children with mild traumatic brain injury versus orthopedic injury. J Neurotrauma 2020;37(17):1892–1901; doi: 10.1089/neu.2019.6850
16. Mayer AR, Hanlon FM, Ling JM. Gray matter abnormalities in pediatric mild traumatic brain injury. J Neurotrauma 2015;32(10):723–730; doi: 10.1089/neu.2014.3534
17. Ware AL, Yeates KO, Tang K, et al. Longitudinal white matter microstructural changes in pediatric mild traumatic brain injury: an A-CAP study. Hum Brain Mapp 2022;43(12):3809–3823; doi: 10.1002/hbm.25885
18. Garman RH, Jenkins LW, Switzer RC, 3rd, et al. Blast exposure in rats with body shielding is characterized primarily by diffuse axonal injury. J Neurotrauma 2011;28(6):947–959; doi: 10.1089/neu.2010.1540
19. Asken BM, DeKosky ST, Clugston JR, et al. Diffusion tensor imaging (DTI) findings in adult civilian, military, and sport-related mild traumatic brain injury (mTBI): a systematic critical review. Brain Imaging Behav 2018;12(2):585–612; doi: 10.1007/s11682-017-9708-9
20. Hannawi Y, Stevens RD. Mapping the connectome following traumatic brain injury. Curr Neurol Neurosci Rep 2016;16(5):44; doi: 10.1007/s11910-016-0642-9
21. Dennis EL, Babikian T, Giza CC, et al. Diffusion MRI in pediatric brain injury. Childs Nerv Syst 2017;33(10):1683–1692; doi: 10.1007/s00381-017-3522-y
22. Alhilali LM, Delic JA, Gumus S, et al. Evaluation of white matter injury patterns underlying neuropsychiatric symptoms after mild traumatic brain injury. Radiology 2015;277(3):793–800; doi: 10.1148/radiol.2015142974
23. Borich M, Makan N, Boyd L, et al. Combining whole-brain voxel-wise analysis with in vivo tractography of diffusion behavior after sports-related concussion in adolescents: a preliminary report. J Neurotrauma 2013;30(14):1243–1249; doi: 10.1089/neu.2012.2818
24. Chu Z, Wilde EA, Hunter JV, et al. Voxel-based analysis of diffusion tensor imaging in mild traumatic brain injury in adolescents. Am J Neuroradiol 2010;31(2):340–346; doi: 10.3174/ajnr.A1806

25. Fakhran S, Yaeger K, Collins M, et al. Sex differences in white matter abnormalities after mild traumatic brain injury: localization and correlation with outcome. Radiology 2014;272(3):815–823; doi: 10.1148/radiol.14132512
26. King R, Grohs MN, Kirton A, et al. Microstructural neuroimaging of white matter tracts in persistent post-concussion syndrome: a prospective controlled cohort study. NeuroImage Clin 2019;23:101842; doi: 10.1016/j.nicl.2019.101842
27. Manning KY, Schranz A, Bartha R, et al. Multiparametric MRI changes persist beyond recovery in concussed adolescent hockey players. Neurology 2017;89(21):2157–2166; doi: 10.1212/wnl.0000000000004669
28. Mayer AR, Ling JM, Yang Z, et al. Diffusion abnormalities in pediatric mild traumatic brain injury. J Neuroscience 2012;32(50):17961–17969; doi: 10.1523/jneurosci.3379-12.2012
29. van Beek L, Ghesquiere P, Lagae L, et al. Mathematical difficulties and white matter abnormalities in sub-acute pediatric mild traumatic brain injury. J Neurotrauma 2015;32(20):1567–1578; doi: 10.1089/neu.2014.3809
30. Wilde EA, McCauley SR, Hunter JV, et al. Diffusion tensor imaging of acute mild traumatic brain injury in adolescents. Neurology 2008;70(12):948–955; doi: 10.1212/01.wnl.0000305961.68029.54
31. Wilde EA, Ware AL, Li X, et al. Orthopedic injured versus uninjured comparison groups for neuroimaging research in mild traumatic brain onjury. J Neurotrauma 2019;36(2):239–249; doi: 10.1089/neu.2017.5513
32. Wu TC, Wilde EA, Bigler ED, et al. Evaluating the relationship between memory functioning and cingulum bundles in acute mild traumatic brain injury using diffusion tensor imaging. J Neurotrauma 2010;27(2):303–307; doi: 10.1089/neu.2009.1110
33. Yallampalli R, Wilde EA, Bigler ED, et al. Acute white matter differences in the fornix following mild traumatic brain injury using diffusion tensor imaging. J Neuroimaging 2013;23(2):224–227; doi: 10.1111/j.1552-6569.2010.00537.x
34. Babcock L, Yuan W, Leach J, et al. White matter alterations in youth with acute mild traumatic brain injury. J Pediatr Rehabil Med 2015;8(4):285–296; doi: 10.3233/prm-150347
35. Virji-Babul N, Borich MR, Makan N, et al. Diffusion tensor imaging of sports-related concussion in adolescents. Pediatric Neurol 2013;48(1):24–29; doi: 10.1016/j.pediatrneurol.2012.09.005
36. Yuan W, Wade SL, Babcock L. Structural connectivity abnormality in children with acute mild traumatic brain injury using graph theoretical analysis. Human Brain Mapp 2015;36(2):779–792; doi: 10.1002/hbm.22664
37. Yuan W, Wade SL, Quatman-Yates C, et al. Structural connectivity related to persistent symptoms after mild TBI in adolescents and response to aerobic training: preliminary investigation. J Head Trauma Rehabil 2017;32(6):378–384; doi: 10.1097/HTR.0000000000000318
38. Delic J, Alhilali LM, Hughes MA, et al. White matter injuries in mild traumatic brain injury and posttraumatic migraines: diffusion entropy analysis. Radiology 2016;279(3):859–866; doi: 10.1148/radiol.2015151388
39. Maugans TA, Farley C, Altaye M, et al. Pediatric sports-related concussion produces cerebral blood flow alterations. Pediatrics 2012;129(1):28–37; doi: 10.1542/peds.2011-2083
40. Satchell EK, Friedman SD, Bompadre V, et al. Use of diffusion tension imaging in the evaluation of pediatric concussions. Musculoskelet Sci Pract 2019;42:162–165; doi: 10.1016/j.msksp.2019.05.002
41. Ware AL, Shukla A, Goodrich-Hunsaker NJ, et al. 7. NeuroImage Clin 2020;25:102106; doi: 10.1016/j.nicl.2019.102106
42. Wu T, Merkley TL, Wilde EA, et al. A preliminary report of cerebral white matter microstructural changes associated with adolescent sports concussion acutely and sub-acutely using diffusion tensor imaging. Brain Imaging Behav 2018;12(4):962–973; doi: 10.1007/s11682-017-9752-5
43. Lancaster MA, Meier TB, Olson DV, et al. Chronic differences in white matter integrity following sport-related concussion as measured by diffusion MRI: 6-month follow-up. Human Brain Mapp 2018;39(11):4276–4289; doi: 10.1002/hbm.24245
44. Murdaugh DL, King TZ, Sun B, et al. Longitudinal changes in resting state connectivity and white matter integrity in adolescents with sports-related concussion. J Int Neuropsychol Soc 2018;24(8):781–792; doi: 10.1017/s1355617718000413
45. Davenport EM, Whitlow CT, Urban JE, et al. Abnormal white matter integrity related to head impact exposure in a season of high school varsity football. J Neurotrauma 2014;31(19):1617–1624; doi: 10.1089/neu.2013.3233
46. Abbas K, Shenk TE, Poole VN, et al. Alteration of default mode network in high school football athletes due to repetitive subconcussive mild traumatic brain injury: a resting-state functional magnetic resonance imaging study. Brain Connect 2015;5(2):91–101; doi: 10.1089/brain.2014.0279
47. Borich M, Babul AN, Yuan PH, et al. Alterations in resting-state brain networks in concussed adolescent athletes. J Neurotrauma 2015;32(4):265–271; doi: 10.1089/neu.2013.3269
48. Stephenson DD, Meier TB, Pabbathi Reddy S, et al. Resting-state power and regional connectivity after pediatric mild traumatic brain injury. J Magn Reson Imaging 2020; 52(6):1701–1713; doi: 10.1002/jmri.27249
49. Vaughn KA, DeMaster D, Kook JH, et al. Effective connectivity in the default mode network after paediatric traumatic brain injury. Eur J Neurosci 2022;55(1):318–336; doi: 10.1111/ejn.15546
50. Huang MX, Robb Swan A, Angeles Quinto A, et al. Resting-state magnetoencephalography source imaging pilot study in children with mild traumatic brain injury. J Neurotrauma 2020;37(7):994–1001; doi: 10.1089/neu.2019.6417
51. Lima Santos JP, Kontos AP, Mailliard S, et al. White matter abnormalities associated with prolonged recovery in adolescents following concussion. Front Neurol 2021;12:681467; doi: 10.3389/fneur.2021.681467
52. Emery CA, Barlow KM, Brooks BL, et al. A systematic review of psychiatric, psychological, and behavioural outcomes following mild traumatic brain injury in children and adolescents. Can J Psychiatry 2016;61(5):259–269; doi: 10.1177/0706743716643741
53. Bigler ED, Abildskov TJ, Goodrich-Hunsaker NJ, et al. Structural neuroimaging findings in mild traumatic brain injury. Sports Med Arthrosc Rev 2016;24(3):e42–e52; doi: 10.1097/JSA.0000000000000119
54. Huang MX, Harrington DL, Robb Swan A, et al. Resting-state magnetoencephalography reveals different patterns of aberrant functional connectivity in combat-related mild traumatic brain injury. J Neurotrauma 2017;34(7):1412–1426; doi: 10.1089/neu.2016.4581
55. Huang MX, Nichols S, Baker DG, et al. Single-subject-based whole-brain MEG slow-wave imaging approach for detecting abnormality in patients with mild traumatic brain injury. NeuroImage Clin 2014;5:109–119; doi: 10.1016/j.nicl.2014.06.004
56. Huang MX, Nichols S, Robb A, et al. An automatic MEG low-frequency source imaging approach for detecting injuries in mild and moderate TBI patients with blast and non-blast causes. NeuroImage 2012;61(4):1067–1082; doi: 10.1016/j.neuroimage.2012.04.029
57. Kaltiainen H, Helle L, Liljestrom M, et al. Theta-band oscillations as an indicator of mild traumatic brain injury. Brain Topogr 2018;31(6):1037–1046; doi: 10.1007/s10548-018-0667-2
58. Tarapore PE, Findlay AM, Lahue SC, et al. Resting state magnetoencephalography functional connectivity in traumatic brain injury. J Neurosurg 2013;118(6):1306–1316; doi: 10.3171/2013.3.JNS12398
59. Krieger D, Shepard P, Soose R, et al. Symptom-dependent changes in MEG-derived neuroelectric brain activity in traumatic brain injury patients with chronic symptoms. Med Sci (Basel) 2021;9(2); doi: 10.3390/medsci9020020
60. Krieger D, Shepard P, Soose R, et al. MEG-derived symptom-sensitive biomarkers with long-term test-retest reliability. Diagnostics (Basel) 2021;12(1); doi: 10.3390/diagnostics12010084
61. Vascak M, Jin X, Jacobs KM, et al. Mild traumatic brain injury induces structural and functional disconnection of local neocortical inhibitory networks via parvalbumin interneuron diffuse axonal injury. Cereb Cortex 2018;28(5):1625–1644; doi: 10.1093/cercor/bhx058
62. Robb Swan A, Nichols S, Drake A, et al. Magnetoencephalography slow-wave detection in patients with mild traumatic brain injury and ongoing symptoms correlated with long-term neuropsychological outcome. J Neurotrauma 2015;32(19):1510–1521; doi: 10.1089/neu.2014.3654
63. Leahy RM, Mosher JC, Spencer ME, et al. A study of dipole localization accuracy for MEG and EEG using a human skull phantom. Electroencephalogr Clin Neurophysiol 1998;107(2):159–73; doi: 10.1016/s0013-4694(98)00057-1
64. Hamalainen MS, Hari R, Ilmoniemi RJ, et al. Magnetoencephalography—theory, instrumentation, and applications to noninvasive studies of the working human brain. Rev Modern Physics 1993;65:413–497
65. Lewine JD, Davis JT, Bigler ED, et al. Objective documentation of traumatic brain injury subsequent to mild head trauma: multimodal brain imaging with MEG, SPECT, and MRI. J head Trauma Rehabil 2007;22(3):141–155; doi: 10.1097/01.HTR.0000271115.29954.27
66. Lewine JD, Davis JT, Sloan JH, et al. Neuromagnetic assessment of pathophysiologic brain activity induced by minor head trauma. AJNR Am J Neuroradiol 1999;20(5):857–866

67. Huang MX, Huang CW, Harrington DL, et al. Marked increases in resting-state MEG gamma-band activity in combat-related mild traumatic brain injury. Cereb Cortex 2020;30(1):283–295; doi: 10.1093/cercor/bhz087
68. Huang MX, Nichols S, Robb-Swan A, et al. MEG Working memory N-back task reveals functional deficits in combat-related mild traumatic brain injury. Cereb Cortex 2019;29(5):1953–1968; doi: 10.1093/cercor/bhy075
69. Vakorin VA, Doesburg SM, da Costa L, et al. Detecting mild traumatic brain injury using resting state magnetoencephalographic connectivity. PLoS Comput Biol 2016;12(12):e1004914; doi: 10.1371/journal.pcbi.1004914
70. Dimitriadis SI, Zouridakis G, Rezaie R, et al. Functional connectivity changes detected with magnetoencephalography after mild traumatic brain injury. NeuroImage Clin 2015;9:519–531; doi: 10.1016/j.nicl.2015.09.011
71. Teasdale G, Jennett B. Assessment of coma and impaired consciousness. A practical scale. Lancet 1974;2(7872):81–84; doi: 10.1016/s0140-6736(74)91639-0
72. Association for the Advancement of Automotive Medicine. Abbreviated Injury Scale, 1990 Revision. Association for the Advancement of Automotive Medicine: Des Plaines, IL; 1990.
73. Niedermeyer E, Lopes da Silva FH. Electroencephalography: Basic Principles, Clinical Applications, and Related Fields. Lippincott Williams & Wilkins: Philadelphia, PA; 2005.
74. Ayr LK, Yeates KO, Taylor HG, et al. Dimensions of postconcussive symptoms in children with mild traumatic brain injuries. J Int Neuropsychol Soc 2009;15(1):19–30; doi: 10.1017/S1355617708090188
75. McCauley SR, Wilde EA, Anderson VA, et al. Recommendations for the use of common outcome measures in pediatric traumatic brain injury research. J Neurotrauma 2012;29(4):678–705; doi: 10.1089/neu.2011.1838
76. O'Brien H, Minich NM, Langevin LM, et al. Normative and psychometric Ccharacteristics of the health and behavior inventory among children with mild orthopedic injury presenting to the emergency department: implications for assessing postconcussive symptoms using the child Sport Concussion Assessment Tool 5th Edition (Child SCAT5). Clin J Sport Med 2021;31(5):e221–e228; doi: 10.1097/JSM.0000000000000943
77. Bernard CO, Ponsford JL, McKinlay A, et al. Do concussive symptoms really resolve in young children? J Head trauma Rehabil 2017;32(6):413–424; doi: 10.1097/HTR.0000000000000298
78. Cohen D, Schlapfer U, Ahlfors S, et al. New Six-Layer Magnetically-Shielded Room for MEG. VDE Verlag: Jena, Germany; 2002.
79. Oken BS, Salinsky MC, Elsas SM. Vigilance, alertness, or sustained attention: physiological basis and measurement. Clin Neurophysiol 2006;117(9):1885–1901; doi: 10.1016/j.clinph.2006.01.017
80. Song T, Gaa K, Cui L, et al. Evaluation of signal space separation via simulation. Med Biol Eng Comput 2008;46(9):923–932; doi: 10.1007/s11517-007-0290-y
81. Taulu S, Kajola M, Simola J. Suppression of interference and artifacts by the Signal Space Separation Method. Brain Topogr 2004;16(4):269–275; doi: 10.1023/b:brat.0000032864.93890.f9
82. Taulu S, Simola J, Kajola M. MEG recordings of DC fields using the signal space separation method (SSS). Neurol Clin Neurophysiol 2004;2004:35.
83. Hyvarinen A. Fast and robust fixed-point algorithms for independent component analysis. IEEE Trans Neural Netw 1999;10(3):626–634; doi: 10.1109/72.761722
84. Hyvarinen A, Oja E. Independent component analysis: algorithms and applications. Neural Netw 2000;13(4-5):411–430; doi: 10.1016/s0893-6080(00)00026-5
85. Jovicich J, Czanner S, Greve D, et al. Reliability in multi-site structural MRI studies: effects of gradient non-linearity correction on phantom and human data. NeuroImage 2006;30(2):436–443; doi: 10.1016/j.neuroimage.2005.09.046
86. Huang MX, Song T, Hagler DJ, Jr., et al. A novel integrated MEG and EEG analysis method for dipolar sources. NeuroImage 2007;37(3):731–748; doi: 10.1016/j.neuroimage.2007.06.002
87. Mosher JC, Leahy RM, Lewis PS. EEG and MEG: forward solutions for inverse methods. IEEE Trans Biomed Eng 1999;46(3):245–259; doi: 10.1109/10.748978
88. Huang MX, Huang CW, Robb A, et al. MEG source imaging method using fast L1 minimum-norm and its applications to signals with brain noise and human resting-state source amplitude images. NeuroImage 2014;84:585–604; doi: 10.1016/j.neuroimage.2013.09.022
89. Huang CW, Huang MX, Ji Z, et al. High-resolution MEG source imaging approach to accurately localize Broca's area in patients with brain tumor or epilepsy. Clin Neurophysiol 2016;127(5):2308–2316; doi: 10.1016/j.clinph.2016.02.007
90. Grabner G, Janke AL, Budge MM, et al. Symmetric atlasing and model based segmentation: an application to the hippocampus in older adults. Med Image Comput Comput Assist Interv 2006;9(Pt 2):58–66; doi: 10.1007/11866763_8
91. Smith SM, Jenkinson M, Woolrich MW, et al. Advances in functional and structural MR image analysis and implementation as FSL. NeuroImage 2004;23 Suppl 1:S208–S219; doi: 10.1016/j.neuroimage.2004.07.051
92. Woolrich MW, Jbabdi S, Patenaude B, et al. Bayesian analysis of neuroimaging data in FSL. NeuroImage 2009;45(1 Suppl):S173–S186; doi: 10.1016/j.neuroimage.2008.10.055
93. Shen X, Tokoglu F, Papademetris X, et al. Groupwise whole-brain parcellation from resting-state fMRI data for network node identification. NeuroImage 2013;82:403–415; doi: 10.1016/j.neuroimage.2013.05.081
94. Ji S, Yang M, Yu K. 3D convolutional neural networks for human action recognition. IEEE Trans Pattern Anal Mach Intell 2013;35(1):221–231; doi: 10.1109/TPAMI.2012.59
95. Eo T, Jun Y, Kim T, et al. KIKI-net: cross-domain convolutional neural networks for reconstructing undersampled magnetic resonance images. Magn Reson Med 2018;80(5):2188–2201; doi: 10.1002/mrm.27201
96. Hammernik K, Klatzer T, Kobler E, et al. Learning a variational network for reconstruction of accelerated MRI data. Magn Reson Med 2018;79(6):3055–3071; doi: 10.1002/mrm.26977
97. Hyun CM, Kim HP, Lee SM, et al. Deep learning for undersampled MRI reconstruction. Phys Med Biol 2018;63(13):135007; doi: 10.1088/1361-6560/aac71a
98. Jun Y, Eo T, Shin H, et al. Parallel imaging in time-of-flight magnetic resonance angiography using deep multistream convolutional neural networks. Magn Reson Med 2019;81(6):3840–3853; doi: 10.1002/mrm.27656
99. Kwon K, Kim D, Park H. A parallel MR imaging method using multilayer perceptron. Med Phys 2017;44(12):6209–6224; doi: 10.1002/mp.12600
100. Yang G, Yu S, Dong H, et al. DAGAN: Deep de-aliasing generative adversarial networks for fast compressed sensing MRI reconstruction. IEEE Trans Med Imaging 2018;37(6):1310-–1321; doi: 10.1109/TMI.2017.2785879
101. Lu X, Yang Y, Wu F, et al. Discriminative analysis of schizophrenia using support vector machine and recursive feature elimination on structural MRI images. Medicine (Baltimore) 2016;95(30):e3973; doi: 10.1097/MD.0000000000003973
102. Muller AC, Guido S. Introduction to Machine Learning with Python. O'Reilly Media, Inc.: Sebastopol, CA; 2016.
103. Wang C, Xiao Z, Wu J. Functional connectivity-based classification of autism and control using SVM-RFECV on rs-fMRI data. Phys Med 2019;65:99–105; doi: 10.1016/j.ejmp.2019.08.010
104. Shao J. Linear model selection by cross-validation. J Am Stat Assoc 1993;88(486-494)
105. James A, Witten D, Hastie T, et al. An Introduction to Statistical Learning with Applications in R. Springer: New York, NY; 2021.
106. Xu QS, Liang YZ. Monte Carlo cross-validation. Chemom Intell Lab Syst 2004;56(1):1–11; https://doi.org/10.1016/S0169-7439(00)00122-2
107. Xu QS, Liang YZ, Du YP. Monte Carlo cross-validation for selecting a model and estimating the prediction error in multivariate calibration. J Chemom 2004;18(2):112–120; https://doi.org/10.1002/cem.858
108. Wechsler D. Weschler Abbreviated Scale of Intelligence Manual. The Psychological Corporation: San Antonio, TX; 2011.
109. Papa L, Edwards D, Ramia M. Exploring serum biomarkers for mild traumatic brain injury. In: Brain Neurotrauma: Molecular, Neuropsychological, and Rehabilitation Aspects. (Kobeissy FH. ed.) CRC Press/-Taylor & Francis: Boca Raton (FL); 2015.
110. Giza CC, Hovda DA. The new neurometabolic cascade of concussion. Neurosurgery 2014;75 Suppl 4:S24–S33; doi: 10.1227/NEU.0000000000000505
111. Gloor P, Ball G, Schaul N. Brain lesions that produce delta waves in the EEG. Neurology 1977;27(4):326–333; doi: 10.1212/wnl.27.4.326
112. Ball GJ, Gloor P, Schaul N. The cortical electromicrophysiology of pathological delta waves in the electroencephalogram of cats. Electroencephalogr Clin Neurophysiol 1977;43(3):346–361; doi: 10.1016/0013-4694(77)90258-9

113. Schaul N, Gloor P, Ball G, et al. The electromicrophysiology of delta waves induced by systemic atropine. Brain Res 1978;143(3):475–486; doi: 10.1016/0006-8993(78)90358-x
114. Schaul N. The fundamental neural mechanisms of electroencephalography. Electroencephalogr Clin Neurophysiol 1998;106(2):101–107; doi: 10.1016/s0013-4694(97)00111-9
115. Hsieh TH, Lee HHC, Hameed MQ, et al. Trajectory of parvalbumin cell impairment and loss of cortical inhibition in traumatic brain injury. Cereb Cortex 2017;27(12):5509–5524; doi: 10.1093/cercor/bhw318
116. Carlen M, Meletis K, Siegle JH, et al. A critical role for NMDA receptors in parvalbumin interneurons for gamma rhythm induction and behavior. Mol Psychiatry 2012;17(5):537–548; doi: 10.1038/mp.2011.31
117. Traub RD, Whittington MA, Stanford IM, et al. A mechanism for generation of long-range synchronous fast oscillations in the cortex. Nature 1996;383(6601):621–624; doi: 10.1038/383621a0
118. Cardin JA, Carlen M, Meletis K, et al. Driving fast-spiking cells induces gamma rhythm and controls sensory responses. Nature 2009;459(7247):663–667; doi: 10.1038/nature08002
119. Fries P. Neuronal gamma-band synchronization as a fundamental process in cortical computation. Ann Rev Neurosci 2009;32:209–224; doi: 10.1146/annurev.neuro.051508.135603
120. Sohal VS, Zhang F, Yizhar O, et al. Parvalbumin neurons and gamma rhythms enhance cortical circuit performance. Nature 2009;459(7247):698–702; doi: 10.1038/nature07991
121. Cho KK, Hoch R, Lee AT, et al. Gamma rhythms link prefrontal interneuron dysfunction with cognitive inflexibility in Dlx5/6(+/-) mice. Neuron 2015;85(6):1332–1343; doi: 10.1016/j.neuron.2015.02.019
122. Kalemaki K, Konstantoudaki X, Tivodar S, et al. Mice with decreased number of interneurons exhibit aberrant spontaneous and oscillatory activity in the cortex. Front Neural Circuits 2018;12:96; doi: 10.3389/fncir.2018.00096
123. Del Pino I, Garcia-Frigola C, Dehorter N, et al. Erbb4 deletion from fast-spiking interneurons causes schizophrenia-like phenotypes. Neuron 2013;79(6):1152–1168; doi: 10.1016/j.neuron.2013.07.010
124. Korotkova T, Fuchs EC, Ponomarenko A, et al. NMDA receptor ablation on parvalbumin-positive interneurons impairs hippocampal synchrony, spatial representations, and working memory. Neuron 2010;68(3):557–569; doi: 10.1016/j.neuron.2010.09.017
125. Rier L, Zamyadi R, Zhang J, et al. Mild traumatic brain injury impairs the coordination of intrinsic and motor-related neural dynamics. NeuroImage Clin 2021;32:102841; doi: 10.1016/j.nicl.2021.102841
126. Huang MX, Huang CW, Harrington DL, et al. Resting-state magnetoencephalography source magnitude imaging with deep-learning neural network for classification of symptomatic combat-related mild traumatic brain injury. Hum Brain Mapp 2021, 42(7):1987–2004; doi: 10.1002/hbm.25340
127. Risen SR, Barber AD, Mostofsky SH, et al. Altered functional connectivity in children with mild to moderate TBI relates to motor control. J Pediatric Eehabil Med 2015;8(4):309–319; doi: 10.3233/prm-150349
128. Caeyenberghs K, Wenderoth N, Smits-Engelsman BC, et al. Neural correlates of motor dysfunction in children with traumatic brain injury: exploration of compensatory recruitment patterns. Brain 2009;132(Pt 3):684–694; doi: 10.1093/brain/awn344
129. Tuerk C, Degeilh F, Catroppa C, et al. Altered resting-state functional connectivity within the developing social brain after pediatric traumatic brain injury. Hum Brain Mapp 2020;41(2):561-576; doi: 10.1002/hbm.24822
130. Xiao H, Yang Y, Xi JH, et al. Correction: Structural and functional connectivity in traumatic brain injury. Neural Regen Res 2017;12(10):1562; doi: 10.4103/1673-5374.217356
131. Xiao H, Yang Y, Xi JH, et al. Structural and functional connectivity in traumatic brain injury. Neural Regen Res 2015;10(12):2062–2071; doi: 10.4103/1673-5374.172328
132. Bonnelle V, Leech R, Kinnunen KM, et al. Default mode network connectivity predicts sustained attention deficits after traumatic brain injury. J Neurosci 2011;31(38):13442–13451; doi: 10.1523/JNEUROSCI.1163-11.2011
133. Botchway E, Kooper CC, Pouwels PJW, et al. Resting-state network organisation in children with traumatic brain injury. Cortex 2022;154:89–104; doi: 10.1016/j.cortex.2022.05.014
134. Mayer AR, Stephenson DD, Dodd AB, et al. Comparison of Methods for Classifying Persistent Post-Concussive Symptoms in Children. J Neurotrauma 2020;37(13):1504–1511; doi: 10.1089/neu.2019.6805
135. Kaufman J, Birmaher B, Axelson D, et al. Kiddie Schedule for Affective Disorders and Schizophrenia—Present and Lifetime Version 2013: Working Draft. Yale University: New Haven, CT.; 2013.
136. Baillet S. Magnetoencephalography for brain electrophysiology and imaging. Nature Neurosci 2017;20(3):327–339; doi: 10.1038/nn.4504
137. Tierney TM, Holmes N, Mellor S, et al. Optically pumped magnetometers: From quantum origins to multi-channel magnetoencephalography. NeuroImage 2019;199:598–608; doi: 10.1016/j.neuroimage.2019.05.063
138. Shah VK, Wakai RT. A compact, high performance atomic magnetometer for biomedical applications. Phys Med Biol 2013;58(22):8153–8161; doi: 10.1088/0031-9155/58/22/8153
139. Boto E, Holmes N, Leggett J, et al. Moving magnetoencephalography towards real-world applications with a wearable system. Nature 2018;555(7698):657–661; doi: 10.1038/nature26147
140. Boto E, Meyer SS, Shah V, et al. A new generation of magnetoencephalography: Room temperature measurements using optically-pumped magnetometers. NeuroImage 2017;149:404–414; doi: 10.1016/j.neuroimage.2017.01.034